*J. Fluid Mech.* (2013), *vol.* 737, *pp.* 552–570.  
doi:10.1017/jfm.2013.581

# A trajectory equation for walking droplets: hydrodynamic pilot-wave theory

**Anand U. Oza, Rodolfo R. Rosales and John W. M. Bush†**

Department of Mathematics, Massachusetts Institute of Technology, Cambridge, MA 02139, USA

(Received 24 May 2013; revised 23 August 2013; accepted 28 October 2013)

We present the results of a theoretical investigation of droplets bouncing on a vertically vibrating fluid bath. An integro-differential equation describing the horizontal motion of the drop is developed by approximating the drop as a continuous moving source of standing waves. Our model indicates that, as the forcing acceleration is increased, the bouncing state destabilizes into steady horizontal motion along a straight line, a walking state, via a supercritical pitchfork bifurcation. Predictions for the dependence of the walking threshold and drop speed on the system parameters compare favourably with experimental data. By considering the stability of the walking state, we show that the drop is stable to perturbations in the direction of motion and neutrally stable to lateral perturbations. This result lends insight into the possibility of chaotic dynamics emerging when droplets walk in complex geometries.

**Key words:** drops, Faraday waves, waves/free-surface flows

## 1. Introduction

In a remarkable series of recent experiments, Yves Couder and coworkers have demonstrated phenomena reminiscent of quantum mechanics in a macroscopic hydrodynamic system (Eddi *et al.* 2009; Couder & Fort 2006; Fort *et al.* 2010). Specifically, they have discovered that millimetric droplets walking on a vibrating fluid bath exhibit several features previously thought to be peculiar to the microscopic quantum realm (Bush 2010). Eddi *et al.* (2009) demonstrated that the droplets can 'tunnel' across shallow fluid regions where walking is forbidden, which is reminiscent of electrons tunnelling through classically forbidden regions of space. Fort *et al.* (2010) observed orbital quantization of walkers on a rotating fluid bath, and developed an analogy between the drop's quantized orbits and the Landau levels of an electron in a uniform magnetic field. Eddi *et al.* (2012) demonstrated that pairs of walkers orbiting in a rotating frame exhibit orbital level splitting. Couder & Fort (2006) explored hydrodynamic analogues of particle diffraction in single- and double-slit geometries by directing walkers towards gaps between submerged barriers. Harris *et al.* (2013) examined the statistics of walking droplets confined to a circular cavity, a hydrodynamic analogue of a quantum corral (Crommie, Lutz & Eigler 1993). In both the diffraction and corral experiments, the complex walker dynamics may give rise to a coherent statistical behaviour with wave-like features. We here develop an

† Email address for correspondence: bush@math.mit.edu

integro-differential trajectory equation for these walking droplets with a view to gaining insight into their subtle dynamics.

Consider a fluid bath vibrating vertically with acceleration $\gamma \cos \omega t$, where $\omega = 2\pi f$. When $\gamma$ is increased beyond $\gamma_F$, the fluid surface goes unstable to a standing field of Faraday waves. The critical acceleration $\gamma_F$, the Faraday threshold, depends on the fluid viscosity, depth, and surface tension. At the onset of instability, subharmonic waves with frequency $\omega/2$ emerge; at higher $\gamma$, higher harmonics of frequency $n\omega/2$ (for integer $n$) can arise. This system was first examined by Faraday (1831), and has since been explored by many others (Douady 1990; Miles & Henderson 1990; Müller, Friedrich & Papathanassiou 1998). A theoretical description of Faraday waves was developed for inviscid fluids by Benjamin & Ursell (1954) and extended to the case of viscous fluids by Kumar (1996). In this paper, we will only consider the regime $\gamma < \gamma_F$, for which the flat interface would be stable if not for the presence of a drop.

Walker (1978) demonstrated that droplets can be made to bounce indefinitely at frequency $\omega$ on the surface of a vertically vibrating bath of the same fluid. When $\gamma < \gamma_B$, $\gamma_B$ being the bouncing threshold, the drop simply coalesces with the fluid bath; however, for $\gamma > \gamma_B$, coalescence is precluded by the sustenance of an air layer between the drop and bath for the duration of the drop impact (Couder, Gautier & Boudaoud 2005). The first theoretical examination of the bouncing process is presented by Couder *et al.* (2005) and built upon by Moláček & Bush (2013*a*). In summary, the drop bounces provided its contact time is less than the time required for the air layer between the drop and bath to drain to a critical thickness of approximately 50 nm, at which coalescence is initiated. Moláček & Bush (2013*a*) developed a complete theoretical description of the bouncing drop dynamics that provides a rationale for all reported periodic and chaotic bouncing states (Wind-Willassen *et al.* 2013).

Protière, Boudaoud & Couder (2006) demonstrate that, as $\gamma$ is increased beyond $\gamma_B$, the drop undergoes a sequence of bifurcations. First, the drop undergoes a period-doubling transition, after which it bounces at frequency $\omega/2$. Its bouncing frequency is then commensurate with the frequency of the least stable Faraday mode, which is thus locally excited through the resonant interaction between drop and bath. For $\gamma > \gamma_W > \gamma_B$, $\gamma_W$ being the walking threshold, the waves generated by the drop destabilize the bouncing state. If the drop is perturbed in some direction, it lands on a sloping interface and so receives a horizontal force on impact that propels it forward. In certain parameter regimes delineated by Protière *et al.* (2006) and Eddi *et al.* (2008) and rationalized by Moláček & Bush (2013*b*), the resulting walking state is quite robust: the drop can walk steadily and stably at a uniform horizontal velocity while bouncing vertically at frequency $\omega/2$. Images of a walking drop and its associated wave field are shown in figure 1.

The coupled vertical and horizontal dynamics of a walking drop were considered by Moláček & Bush (2013*b*), who elucidated the walker's rich and complex behaviour. For example, the walker may switch between various vertical bouncing modes that coexist for identical system parameters, or walk in an irregular fashion while bouncing chaotically (Wind-Willassen *et al.* 2013). The authors also highlight the importance of the walker's phase with respect to the bath. The amplitude of the waves generated by the drop has a complicated dependence on system parameters through the walker's phase, owing to the coupling between the horizontal and vertical motion. For the sake of simplicity, we consider the special case of 'resonant walkers', for which the drop is in a period-doubled bouncing mode, so its vertical motion is precisely synchronized with the underlying wave. We thus neglect the coupling between the horizontal and

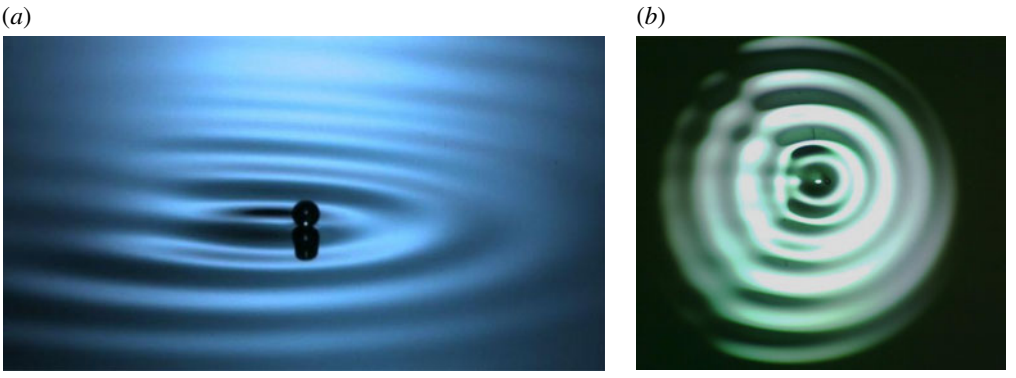


FIGURE 1. (Colour online) A walker, a millimetric droplet, self-propagates on a vibrating fluid bath through an interaction with its own wave field. (*a*) Oblique view. (*b*) Top view.

vertical motion and average over the vertical motion, which allows us to construct and study a trajectory equation for the walker's horizontal motion.

As the propulsive wave force on the walking drop depends on the location of its prior impacts, and so on the walker's past, Fort *et al.* (2010) and Eddi *et al.* (2011) introduced the concept of path-memory. The quantum mechanical features arise only in the high path-memory regime, close to the Faraday threshold, where the waves generated by the walker decay slowly in time and so strongly affect the drop's dynamics (Couder & Fort 2006; Fort *et al.* 2010; Harris *et al.* 2013). In this regime, the drop's trajectory is most strongly influenced by its history, which is effectively stored in the wave field. The goal of the current study is to provide insight into these experiments by developing a trajectory equation for the walkers that illustrates the influence of path-memory on their dynamics.

Protière *et al.* (2006) postulate the following trajectory equation for the horizontal position $x_p$ of the drop, in the absence of barriers and external forces:

$$m\ddot{x}_p + D\dot{x}_p = F^b \sin\left(\frac{2\pi\dot{x}_p}{V_F}\right), \tag{1.1}$$

where $m$ is the drop mass, $F^b$ the effective force due to bouncing on an inclined surface, $D$ the viscous damping coefficient, and $V_F$ the phase velocity of the Faraday waves. Equation (1.1) is derived by time-averaging the horizontal force on the drop over a single bouncing period, and it correctly predicts a supercritical pitchfork bifurcation to a walking state; however, we will see that it only includes the effect of a single previous bounce on the drop's trajectory. A similar approach was taken by Shirokoff (2013) in his theoretical description of walkers in confined geometries. Both papers attempt to model the path-memory through the coefficient $F^b$. We here develop an improved trajectory equation that explicitly models the system's path-memory by incorporating the drop's entire history.

In § 2, we derive an integro-differential equation of motion for the drop by adopting the results presented by Moláček & Bush (2013*b*). The equation indicates that the bouncing state destabilizes at a critical acceleration $\gamma$ into straight-line walking, as shown in § 3. We present an exact formula for the walking speed and compare it to experimental data in § 4, where we also explore the dependence of the guiding wave

field on the walking speed. The stability of the walking solution is analysed in § 5. Future directions and applications of the model are discussed in § 6.

## 2. Integro-differential equation of motion

Consider a drop of mass $m$ and radius $R$ in the presence of a gravitational acceleration $g$ walking on the surface of a vertically vibrating fluid bath of surface tension $\sigma$, density $\rho$, dynamic viscosity $\mu$, kinematic viscosity $\nu$, and mean depth $H$. Let $\boldsymbol{x}_p(t) = (x_p(t), y_p(t))$ denote the horizontal position of the drop at time $t$. We assume that the drop is a resonant walker in the period-doubled regime, so the vertical motion is periodic with period $T_F = 4\pi/\omega$. The force balance in the horizontal direction yields the equation of motion

$$m\ddot{\boldsymbol{x}}_p + D\dot{\boldsymbol{x}}_p = -\overline{F(t)\nabla\mathscr{H}(\boldsymbol{x}_p, t)}, \tag{2.1}$$

where all terms represent time-averages over the bouncing period $T_F$, and $F(t)$ is the vertical force on the drop (Moláček & Bush 2013*b*). The drop moves in response to both propulsive and drag forces. The propulsive force is the wave force imparted by the sloping bath surface during impact. We express the total fluid depth as $H+\mathscr{H}(\boldsymbol{x}, t)$, where we assume the perturbation height $\mathscr{H}(\boldsymbol{x}, t) \ll H$ to be small. The horizontal component of the propulsive force may then be approximated by $-F(t)\nabla\mathscr{H}(\boldsymbol{x}_p, t)$. The drop motion is opposed by a drag force $-D\dot{\boldsymbol{x}}_p$, where the time-averaged drag coefficient $D$ can be written in terms of the system parameters as (Moláček & Bush 2013*b*)

$$D = Cmg\sqrt{\frac{\rho R}{\sigma}} + 6\pi\mu_a R\left(1 + \frac{\pi\rho_a g R}{6\mu_a\omega}\right), \tag{2.2}$$

where $\mu_a = 1.84\times10^{-5}$ kg m$^{-1}$ s$^{-1}$ and $\rho_a = 1.2$ kg m$^{-3}$ are the dynamic viscosity and density of air, and $C$ is the non-dimensional drag coefficient. In (2.2), the first term arises from the transfer of momentum from the drop to the bath during impact, and the second from the aerodynamic drag exerted on the droplet during flight. We note that $C$ actually depends weakly on the system parameters, and $0.17 \leqslant C \leqslant 0.33$ over the parameter range of interest for walkers (Moláček & Bush 2013*b*). For our purposes, it suffices to treat $C = 0.17$ as a constant, a value consistent with the experimental data for $\nu = 20$ cS, $f = 80$ Hz and $\nu = 50$ cS, $f = 50$ Hz (Moláček & Bush 2013*b*).

To determine an expression for the interface deflection $\mathscr{H}(\boldsymbol{x}, t)$, we first consider the interface deflection $h_n(\boldsymbol{x}, t)$ generated by the single bounce of a drop at time $t_n$ and position $\boldsymbol{x}_p(t_n)$. We assume the fluid container to be sufficiently large that we may neglect the influence of boundaries. When the drop hits the surface, it emits a travelling transient wave that is typically an order of magnitude faster than the walker (Eddi *et al.* 2011). We neglect this wave in our model because it does not interact with the drop on subsequent bounces. In the wake of the transient wave, a field of standing waves persists on the interface. Eddi *et al.* (2011) numerically model this standing wave field as

$$h_n(\boldsymbol{x}, t) = \sum_{m=1}^{\infty} a_m(t - t_n)\mathrm{J}_0\left(k_m|\boldsymbol{x} - \boldsymbol{x}_p(t_n)|\right), \tag{2.3}$$

where $\mathrm{J}_0$ is a Bessel function of the first kind, the wavenumbers $k_m$ satisfy the relation $\mathrm{J}_0(k_m r_0) = 0$, and $r_0$ is a numerical cutoff parameter. The time-dependence is

prescribed by the functions $a_m(t)$, which satisfy the equation

$$\ddot{a}_m + 2\nu_{phen}k_m^2\dot{a}_m + a_m\left(g - \gamma\cos\omega t + \frac{\sigma k_m^2}{\rho}\right)k_m\tanh k_m H = 0, \tag{2.4}$$

where $\nu_{phen} \gtrsim \nu$ is the phenomenological kinematic viscosity of the fluid, chosen to match the observed Faraday threshold.

Rather than summing over infinitely many modes, we make some simplifying assumptions that make the model more tractable. Since $\gamma < \gamma_F$, the fluid surface is stable, so all disturbances decay in time. The slowest decaying mode is the subharmonic Faraday wave with temporal decay time $T_F M_e$, where $M_e$ is the non-dimensional memory parameter

$$M_e = M_e(\gamma) \equiv \frac{T_d}{T_F\,(1 - \gamma/\gamma_F)} \tag{2.5}$$

(Eddi *et al.* 2011), and $T_d$ is the temporal decay time in the absence of forcing (Moláček & Bush 2013*b*). In the short-path-memory limit, just above the walking threshold $M_e \gtrsim M_e(\gamma_W)$, the standing waves generated by the drop decay relatively quickly, so the droplet motion depends only on its recent past. In the long-path-memory limit, close to the Faraday threshold $M_e \gg M_e(\gamma_W)$, the standing waves are long-lived, so the walker is more strongly influenced by its history. Both $T_d$ and $\gamma_F$ can be calculated numerically for different fluids and forcing frequencies (Kumar 1996; Moláček & Bush 2013*b*).

The Faraday wave oscillates in time with frequency $\omega/2$, and its dominant wavenumber $k_F$ can be calculated numerically (Kumar 1996; Moláček & Bush 2013*b*) or approximated as the solution to the standard water-wave dispersion relation:

$$\left(\frac{\omega}{2}\right)^2 = \left(gk + \frac{\sigma k^3}{\rho}\right)\tanh kH. \tag{2.6}$$

In the experiments, the Faraday wavenumber is typically $k_F \approx 1.25\ \mathrm{mm}^{-1}$, which corresponds to a Faraday wavelength of $\lambda_F \approx 5$ mm. Fort *et al.* (2010) approximate the Faraday wave generated by a single bounce as

$$h_n(\boldsymbol{x}, t) = \frac{A}{|\boldsymbol{x} - \boldsymbol{x}_p(t_n)|}\cos\left(k_F|\boldsymbol{x} - \boldsymbol{x}_p(t_n)| + \phi\right)\mathrm{e}^{-|\boldsymbol{x}-\boldsymbol{x}_p(t_n)|/\delta}\mathrm{e}^{-(t-t_n)/(T_F M_e)}, \tag{2.7}$$

where the parameters $A$ and $\delta$ are determined experimentally, and $\phi$ is a free parameter. While this model allows them to reproduce many of the experimental results and provides an adequate description in the far field $k_F|\boldsymbol{x} - \boldsymbol{x}_p(t_n)| \gg 1$, it contains a troubling singularity at $\boldsymbol{x} = \boldsymbol{x}_p(t_n)$, and the phase-shifted cosine does not accurately describe the spatial dependence of the Faraday wave near the drop.

Following Moláček & Bush (2013*b*), we approximate the wave as a radial Bessel function of the first kind, $\mathrm{J}_0$, with a single dominant wavenumber $k_F$. This gives the interface height after a single bounce at time $t = t_n$:

$$h_n(\boldsymbol{x}, t) = \tilde{A}\mathrm{J}_0(k_F|\boldsymbol{x} - \boldsymbol{x}_p(t_n)|)\mathrm{e}^{-(t-t_n)/(T_F M_e)}\cos\frac{\omega t}{2}H(t - t_n), \tag{2.8}$$

where $H(t)$ is the Heaviside step function. The amplitude $\tilde{A}$ can be expressed in terms of the system parameters as

$$\tilde{A} = \sqrt{\frac{2}{\pi}} \frac{k_F R}{3k_F^2 R^2 + \mathscr{B}o} \frac{R k_F^2 \nu_{eff}^{1/2}}{\sigma \sqrt{T_F}} mgT_F \sin\frac{\Phi}{2}, \quad \mathscr{B}o = \frac{\rho g R^2}{\sigma}, \quad \nu_{eff} = \nu D_\mu \tag{2.9}$$

where $\mathscr{B}o$ is the Bond number, $\nu_{eff}$ is the effective kinematic viscosity, and $\Phi$ is the mean phase of the wave during the contact time (Moláček & Bush 2013*b*). The coefficient $D_\mu$ is defined as (Prosperetti 1976; Moláček & Bush 2013*b*)

$$D_\mu = -\frac{r_1 + r_2}{2a r_1 r_2} \quad \text{where } a = \frac{\mathscr{O}h (Rk_F)^{3/2}}{\left[\mathscr{B}o + (Rk_F)^2\right]^{1/2}}, \quad \mathscr{O}h = \frac{\mu}{\sqrt{\rho\sigma R}}, \tag{2.10}$$

and $r_1$ and $r_2$ are the roots with largest real part of the polynomial

$$p(x; a) = x^4 + 8ax^3 + (2 + 24a^2)x^2 + a(8 + 16a^2)x + 1 + 8a^2. \tag{2.11}$$

We note that the formula for the interface height (2.8) with amplitude $\tilde{A}$ is an approximation to that given by Moláček & Bush (2013*b*). Here we neglect the $t^{-1/2}$ temporal decay of the waves, as the decay rate is dominated by the exponential $\mathrm{e}^{-(t-t_n)/(T_F M_e)}$. The algebraic factor $t^{-1/2}$ is only valid for $t > T_F$ and makes the governing equation analytically intractable; thus, for the sake of simplicity we replace it by the constant $T_F^{-1/2}$. In addition, we neglect the possibility of multiple vertical bouncing modes for a single forcing acceleration $\gamma$ (Moláček & Bush 2013*b*; Wind-Willassen *et al.* 2013). For a particular bouncing mode, the impact phase $\Phi$ depends in general on $\mu$, $R$, and $\gamma$; however, it depends only weakly on $\gamma$ in the high-memory limit of interest, so we treat it as a constant for a given drop.

We assume the surface waves to be linear, so that we can apply the superposition principle. Thus, the interface height $\mathscr{H}(\boldsymbol{x}, t)$ may be expressed as the sum of the individual waves $h_n(\boldsymbol{x}, t)$ generated by previous bounces at prior times $t_n = nT_F$:

$$\mathscr{H}(\boldsymbol{x}, t) = \sum_n h_n(\boldsymbol{x}, t) = \sum_{n=-\infty}^{\lfloor t/T_F \rfloor} \tilde{A} \mathrm{J}_0(k_F |\boldsymbol{x} - \boldsymbol{x}_p(nT_F)|) \mathrm{e}^{-(t-nT_F)/(T_F M_e)} \cos\frac{\omega t}{2}. \tag{2.12}$$

As shown in Moláček & Bush (2013*b*), since the drop's bouncing period $T_F$ is equal to the period of the surface waves, we may replace $\overline{F(t)\nabla\mathscr{H}(\boldsymbol{x}_p, t)}$ by $mg\nabla h(\boldsymbol{x}_p, t)$, where

$$h(\boldsymbol{x}, t) = \sum_{n=-\infty}^{\lfloor t/T_F \rfloor} A \mathrm{J}_0(k_F |\boldsymbol{x} - \boldsymbol{x}_p(nT_F)|) \mathrm{e}^{-(t-nT_F)/(T_F M_e)}, \quad A = \tilde{A} \cos\frac{\Phi}{2}. \tag{2.13}$$

We call this the *stroboscopic approximation* since, by averaging over the vertical dynamics, we eliminate consideration of the drop's vertical motion. The drop motion is thus effectively 'strobed' at the bouncing frequency.

Substituting (2.13) into (2.1) yields a delay-differential equation of motion for the drop, which is quite difficult to study analytically. We thus approximate the sum in (2.13) by the integral:

$$h(\boldsymbol{x}, t) = \frac{AC_f}{T_F} \int_{-\infty}^{t} \mathrm{J}_0(k_F |\boldsymbol{x} - \boldsymbol{x}_p(s)|) \mathrm{e}^{-(t-s)/(T_F M_e)} \, \mathrm{d}s, \tag{2.14}$$

where $C_f = 1/M_e \left(\mathrm{e}^{1/M_e} - 1\right)$. This approximation is valid provided the time scale of horizontal motion, $T_H = \lambda_F / |\dot{\boldsymbol{x}}_p|$, is much greater than the time scale $T_F$ of vertical

motion, that is, $T_F \ll T_H$, as is the case for walkers. The resonant walker is thus approximated as a continuous moving source of standing waves, and is viewed as sweeping across the fluid interface. We make the additional approximation that $C_f = 1$, since walkers typically arise when $M_e \gg 1$.

Substituting (2.14) into (2.1), we obtain an integro-differential equation of motion:

$$m\ddot{\boldsymbol{x}}_p + D\dot{\boldsymbol{x}}_p = \frac{F}{T_F}\int_{-\infty}^{t} \frac{\mathrm{J}_1(k_F|\boldsymbol{x}_p(t) - \boldsymbol{x}_p(s)|)}{|\boldsymbol{x}_p(t) - \boldsymbol{x}_p(s)|}(\boldsymbol{x}_p(t) - \boldsymbol{x}_p(s))\mathrm{e}^{-(t-s)/(T_F M_e)}\,\mathrm{d}s, \quad (2.15)$$

where $F = mgAk_F$. Note that the equation of motion at time $t$ depends on the drop's entire trajectory prior to that time, on its path memory as stored in the wave field. Nevertheless, the dominant contribution of the integral comes from its recent past, specifically $t - s \sim O(T_F M_e)$. The drop is thus influenced by more of its history as stored in its wave field $h(\boldsymbol{x}, t)$ as its path-memory $M_e$ increases. The term on the right-hand side of (2.15) is thus referred to alternatively as the *wave force* or *memory force*.

The trajectory equation (2.15) is markedly different from that developed by Protière *et al.* (2006), (1.1), which assumes that $h(x, t) = A\cos(k_F(x - x_p(t)))$. By using $V_F = (\omega/2)/k_F$ and $\dot{x}_p(t)T_F \approx x_p(t) - x_p(t - T_F)$ for $T_F \ll 1$, one can obtain from (1.1) the delay-differential equation

$$m\ddot{x}_p + D\dot{x}_p = F^b \sin\left(k_F(x_p(t) - x_p(t - T_F))\right). \quad (2.16)$$

Unlike (2.15), which incorporates the drop's entire history, the model (2.16) only includes the influence of a single prior impact. It can thus be valid only in the short-path-memory limit for walkers just beyond the walking threshold $M_e \gtrsim M_e(\gamma_W)$, and is incapable of capturing the drop dynamics at large $M_e$.

The variables appearing in (2.15) are listed in table 1. Note that the model has no free parameters: formulae for $D$ and $F$ are derived by Moláček & Bush (2013*b*), and $T_d$ and $\gamma_F$ can be determined numerically (Kumar 1996; Moláček & Bush 2013*b*). We proceed by demonstrating that the trajectory equation (2.15) captures certain key aspects of the walker dynamics.

## 3. Bouncing to walking

Note that $\boldsymbol{x}_p \equiv$ constant is a solution to (2.15) that represents a stationary bouncing state. In this section, we will study the stability of this bouncing state, and demonstrate that increasing $M_e$ causes it to destabilize into a walking state, in which the drop moves along a straight line at constant horizontal velocity.

We first non-dimensionalize (2.15). We choose $\lambda_F$ and $T_F M_e$ as our natural length and time scales, respectively, and so non-dimensionalize via $\boldsymbol{x}' = k_F\boldsymbol{x}$ and $t' = t/(T_F M_e)$. Substituting into (2.15) and dropping primes, we deduce the non-dimensional equation of motion:

$$\kappa\ddot{\boldsymbol{x}}_p + \dot{\boldsymbol{x}}_p = \beta\int_{-\infty}^{t} \frac{\mathrm{J}_1(|\boldsymbol{x}_p(t) - \boldsymbol{x}_p(s)|)}{|\boldsymbol{x}_p(t) - \boldsymbol{x}_p(s)|}(\boldsymbol{x}_p(t) - \boldsymbol{x}_p(s))\mathrm{e}^{-(t-s)}\,\mathrm{d}s, \quad (3.1)$$

where $\kappa = m/DT_F M_e$ and $\beta = Fk_F T_F M_e^2/D$ represent, respectively, the non-dimensional mass and memory force coefficient.

| Dimensional variables | Definition |
|---|---|
| $\boldsymbol{x}_p$ | drop position |
| $m$ | drop mass |
| $D$ | drag coefficient |
| $g$ | gravitational acceleration |
| $\mathscr{H}(\boldsymbol{x}, t)$ | interface deflection |
| $T_F$ | Faraday period |
| $\tilde{A}$ | amplitude of single surface wave |
| $k_F$ | Faraday wavenumber |
| $T_d$ | decay time of waves without forcing |
| $\gamma$ | forcing acceleration |
| $\gamma_F$ | Faraday instability threshold |
| $F = mgAk_F$ | memory force coefficient |
| Non-dimensional variables | |
| $M_e = \dfrac{T_d}{T_F(1-\gamma/\gamma_F)}$ | memory |
| $\kappa = \dfrac{m}{DT_F M_e}$ | non-dimensional mass |
| $\beta = \dfrac{Fk_F T_F M_e^2}{D}$ | non-dimensional memory force coefficient |

TABLE 1. The variables appearing in the trajectory equations (2.15) and (3.1).

We now examine the stability of the bouncing solution $\boldsymbol{x}_p \equiv$ constant. By linearizing (3.1) around this solution, $\boldsymbol{x}_p =$ constant $+ \delta\boldsymbol{x}$, we deduce

$$\kappa\delta\ddot{\boldsymbol{x}} + \delta\dot{\boldsymbol{x}} = \frac{\beta}{2}\int_{-\infty}^{t}[\delta\boldsymbol{x}(t) - \delta\boldsymbol{x}(s)]\mathrm{e}^{-(t-s)}\,\mathrm{d}s, \tag{3.2}$$

where we have used the fact that $\mathrm{J}_1'(0) = 1/2$. This equation can be expressed as a system of ordinary differential equations by introducing the variable

$$\delta\boldsymbol{X}(t) = \int_{-\infty}^{t}\delta\boldsymbol{x}(s)\mathrm{e}^{-(t-s)}\,\mathrm{d}s. \tag{3.3}$$

Solutions to (3.2) thus form a subset of solutions to the system of equations

$$\kappa\ddot{\boldsymbol{x}} + \dot{\boldsymbol{x}} = \frac{\beta}{2}(\boldsymbol{x} - \boldsymbol{X}), \quad \dot{\boldsymbol{X}} = \boldsymbol{x} - \boldsymbol{X}. \tag{3.4}$$

Since the $x$ and $y$ directions are uncoupled in this equation, we can simply consider the $x$ direction, the calculation for the $y$ direction being identical. Letting $\dot{x} = u$, we obtain the system

$$\frac{\mathrm{d}}{\mathrm{d}t}\begin{bmatrix} x \\ u \\ X \end{bmatrix} = \begin{bmatrix} 0 & 1 & 0 \\ \dfrac{\beta}{2\kappa} & -\dfrac{1}{\kappa} & -\dfrac{\beta}{2\kappa} \\ 1 & 0 & -1 \end{bmatrix}\begin{bmatrix} x \\ u \\ X \end{bmatrix}. \tag{3.5}$$

The characteristic polynomial $p(s)$ of this matrix is

$$p(s) = -s\left[s^2 + \left(1 + \frac{1}{\kappa}\right)s + \frac{1}{\kappa}\left(1 - \frac{\beta}{2}\right)\right]. \tag{3.6}$$

The $s = 0$ solution simply indicates that the bouncing state is invariant under translation, so we neglect it. Since $\kappa > 0$, the stability of the bouncing state is controlled by the constant term in $p(s)$. Specifically, the bouncing state is stable for $\beta < 2$ and unstable for $\beta > 2$. In terms of the dimensional variables, the bouncing state is stable for forcing accelerations $\gamma < \gamma_W$, where

$$\gamma_W = \gamma_F \left(1 - \sqrt{\frac{Fk_F T_d^2}{2DT_F}}\right) \tag{3.7}$$

defines the walking threshold. Note that $\gamma_W$ increases with the drop drag coefficient $D$ but decreases with the memory force coefficient $F$. Note also that the memory force increases with $\gamma$, as indicated by the definition of the memory parameter $M_e$ (2.5). The bouncing state is thus stabilized by the drag force $-D\dot{\boldsymbol{x}}_p$ (which opposes the drop's motion) and destabilized by the memory force. Once the latter is sufficiently large to overcome the former, the bouncing solution is destabilized, and the drop begins to walk. As we will see in the next section, for $\gamma \gtrsim \gamma_W$ the drop begins to walk at a constant velocity.

### 3.1. *Stuart–Landau equation for the walking velocity*

The experiments of Protière *et al.* (2006) demonstrate that, in a parameter regime delineated by Moláček & Bush (2013*b*), there is a supercritical pitchfork bifurcation at $\gamma = \gamma_W$ (corresponding to $\beta = 2$), where the bouncing state destabilizes into straight-line walking. We proceed by demonstrating that this behaviour is captured by our integro-differential equation of motion, by analysing the drop motion near the bifurcation. Assume that $\gamma$ is slightly above the walking threshold, so $\beta = 2 + \alpha\epsilon^2$ for $0 < \epsilon \ll 1$ and $\alpha > 0$. Near the bifurcation, we can write an asymptotic expansion for $\boldsymbol{x}_p(t)$:

$$\boldsymbol{x}_p(t) = \frac{1}{\epsilon}\boldsymbol{a}(T) + \epsilon^3 \boldsymbol{x}_1(t, T) + O(\epsilon^5), \tag{3.8}$$

where $T = \epsilon^2 t$ is the slow time scale. In what follows, we use the notation $\dot{f} = \partial f/\partial t, f' = \partial f/\partial T$. We substitute this expansion into the non-dimensional equation of motion (3.1) and extract the leading-order terms. Due to the exponential term, the dominant contribution in the integral comes from the region $t - s = O(1)$. Note that

$$\boldsymbol{x}_p(t) - \boldsymbol{x}_p(s) = \epsilon \boldsymbol{a}'(T)(t-s) + \epsilon^3(-\tfrac{1}{2}\boldsymbol{a}''(T)(t-s)^2 + \boldsymbol{x}_1(t, T) - \boldsymbol{x}_1(s, S)) + O(\epsilon^5), \tag{3.9}$$

where $S = \epsilon^2 s$, which gives

$$\begin{aligned} |\boldsymbol{x}_p(t) - \boldsymbol{x}_p(s)|^2 = \epsilon^2 |\boldsymbol{a}'(T)|^2 (t-s)^2 + \epsilon^4 \big[ &-(\boldsymbol{a}'(T) \cdot \boldsymbol{a}''(T))(t-s)^3 \\ &+ 2(t-s)\boldsymbol{a}'(T) \cdot (\boldsymbol{x}_1(t, T) - \boldsymbol{x}_1(s, S))\big] + O(\epsilon^6). \end{aligned} \tag{3.10}$$

Therefore

$$\frac{\mathrm{J}_1(|\boldsymbol{x}_p(t) - \boldsymbol{x}_p(s)|)}{|\boldsymbol{x}_p(t) - \boldsymbol{x}_p(s)|} = \frac{1}{2} - \frac{\epsilon^2}{16}|\boldsymbol{a}'(T)|^2 (t-s)^2 + O(\epsilon^4), \tag{3.11}$$

where we use the fact that $\mathrm{J}_1^{(3)}(0) = -3/8$. The leading-order terms in the integral are thus

$$\int_{-\infty}^{t} \frac{\mathrm{J}_1(|\boldsymbol{x}_p(t) - \boldsymbol{x}_p(s)|)}{|\boldsymbol{x}_p(t) - \boldsymbol{x}_p(s)|} \left(\boldsymbol{x}_p(t) - \boldsymbol{x}_p(s)\right) \mathrm{e}^{-(t-s)}\,\mathrm{d}s$$
$$= \frac{\epsilon}{2}\int_{-\infty}^{t} \boldsymbol{a}'(T)(t-s)\mathrm{e}^{-(t-s)}\,\mathrm{d}s + \frac{\epsilon^3}{2}\int_{-\infty}^{t}\left[-\frac{1}{2}\boldsymbol{a}''(T)(t-s)^2 - \frac{1}{8}\boldsymbol{a}'(T)|\boldsymbol{a}'(T)|^2(t-s)^3\right.$$
$$\left. + (\boldsymbol{x}_1(t,T) - \boldsymbol{x}_1(s,S))\right]\mathrm{e}^{-(t-s)}\,\mathrm{d}s + O(\epsilon^5). \tag{3.12}$$

By changing variables $t - s = z$, we can evaluate some of these integrals. Then using $\beta = 2 + \alpha\epsilon^2$, the equation of motion (3.1) reduces, at leading order, to

$$\kappa\ddot{\boldsymbol{x}}_1 + \dot{\boldsymbol{x}}_1 - \boldsymbol{x}_1 + \int_{-\infty}^{t} \boldsymbol{x}_1(s,S)\mathrm{e}^{-(t-s)}\,\mathrm{d}s = \frac{\alpha}{2}\boldsymbol{a}' - (1+\kappa)\boldsymbol{a}'' - \frac{3}{4}\boldsymbol{a}'|\boldsymbol{a}'|^2. \tag{3.13}$$

Introducing the variable $\boldsymbol{X}_1 = \int_{-\infty}^{t} \boldsymbol{x}_1(s,S)\mathrm{e}^{-(t-s)}\,\mathrm{d}s$, (3.13) can be written in the form

$$\frac{\partial}{\partial t}\left(\kappa\dot{\boldsymbol{x}}_1 + \boldsymbol{x}_1 - \boldsymbol{X}_1\right) = \frac{\alpha}{2}\boldsymbol{a}' - (1+\kappa)\boldsymbol{a}'' - \frac{3}{4}\boldsymbol{a}'|\boldsymbol{a}'|^2. \tag{3.14}$$

In order for the expansion (3.8) to be consistent, $\boldsymbol{x}_1$ should be a bounded function of $t$, which implies that the right side of (3.14) must vanish. This yields an evolution equation for the leading-order velocity $\boldsymbol{a}'$:

$$\boldsymbol{a}'' = \frac{1}{2\,(1+\kappa)}\boldsymbol{a}'\left(\alpha - \frac{3}{2}|\boldsymbol{a}'|^2\right). \tag{3.15}$$

This is a Stuart–Landau equation (Stuart 1958) for the velocity $\boldsymbol{a}'$. We write $\boldsymbol{a}' = u(T)(\cos\theta(T), \sin\theta(T))$, where $u(T)$ is the speed of the drop and $\theta(T)$ determines its direction, so that (3.15) becomes

$$u' = \frac{1}{2\,(1+\kappa)}u\left(\alpha - \frac{3}{2}u^2\right), \quad \theta' = 0. \tag{3.16}$$

We thus confirm that the speed $u$ undergoes a supercritical pitchfork bifurcation when $\beta = 2$. For $\beta < 2$, only the bouncing state $u = 0$ is stable; for $\beta \gtrsim 2$, the walking solution is stable and has speed $u \approx \sqrt{2\alpha/3}$. The equation $\theta' = 0$ implies that, as expected, the drop walks in a straight line in an arbitrary direction: since the wave field produced at each bounce is rotationally symmetric, there is no preferred direction of motion at the onset of instability. Therefore, in the experiment, the initial direction of motion is presumably governed by random or imposed perturbations.

## 4. Straight-line walking

The drop's bouncing state becomes unstable for $\gamma > \gamma_W$, beyond which it walks in a straight line at constant speed. We proceed by deriving a formula for the walking speed of the resonant walker, and showing that the resonant walking state is stable for all $\gamma_W < \gamma < \gamma_F$.

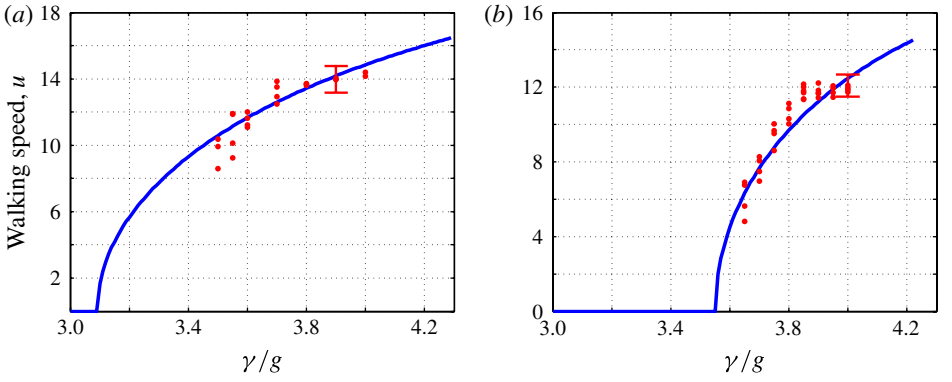


FIGURE 2. (Colour online) Plot of the walking speed $u$ (in mm s$^{-1}$) as a function of the non-dimensional forcing acceleration $\gamma/g$. The dots represent experimental data from Moláček & Bush (2013*b*), and the curves are obtained from our model prediction (4.3) for a resonant walker using (*a*) $\nu = 20$ cS, $f = 80$ Hz, $\rho = 949$ kg m$^{-3}$, $\sigma = 20.6 \times 10^{-3}$ N m$^{-1}$, $\gamma_F = 4.3g$, $T_d = 1/54.9$ s, $R = 0.40$ mm, and (*b*) $\nu = 50$ cS, $f = 50$ Hz, $\rho = 960$ kg m$^{-3}$, $\sigma = 20.8 \times 10^{-3}$ N m$^{-1}$, $\gamma_F = 4.23g$, $T_d = 1/57.9$ s, $R = 0.39$ mm. The single free parameter in our stroboscopic model is the phase of impact, chosen here to be (*a*) $\sin\Phi = 0.3$ and (*b*) $\sin\Phi = 0.35$. Characteristic error bars are shown.

### 4.1. *Walking speed*

To find a formula for the walking speed $u$, we substitute the solution $\boldsymbol{x}_p = (ut, 0)$ into (3.1):

$$u = \beta \int_0^\infty \mathrm{J}_1(uz)\mathrm{e}^{-z}\,\mathrm{d}z. \tag{4.1}$$

The integral can be evaluated exactly, yielding

$$u = \frac{\beta}{u}\left(1 - \frac{1}{\sqrt{1+u^2}}\right) \quad \Rightarrow \quad u = \frac{1}{\sqrt{2}}\left(-1 + 2\beta - \sqrt{1+4\beta}\right)^{1/2}. \tag{4.2}$$

Note that this solution is real-valued only for $\beta > 2$, in accordance with the stability analysis of the bouncing state presented in § 3. In terms of dimensional variables, the walking speed $u$ has the form

$$u = \frac{1}{k_F T_d}\left(1 - \frac{\gamma}{\gamma_F}\right)\left\{\frac{1}{4}\left[-1 + \sqrt{1 + 8\left(\frac{\gamma_F - \gamma_W}{\gamma_F - \gamma}\right)^2}\right]^2 - 1\right\}^{1/2}. \tag{4.3}$$

Figure 2 shows a comparison between the experimental dependence of the walking speed $u$ on the forcing acceleration $\gamma$, as reported by Moláček & Bush (2013*b*), and that predicted by (4.3). The equation for the resonant walking speed adequately describes the experimental data, provided that the impact phase $\Phi$ is judiciously chosen. Note that the impact phases chosen in figure 2 are roughly consistent with those reported in Moláček & Bush (2013*b*); however, they are also known to depend weakly on $\gamma$ (Moláček & Bush 2013*b*).

It follows from (4.3) that $u$ is a monotonically increasing function of $\gamma$. As $\gamma$ increases, so does the propulsive memory force and the drop speed. Moreover, one can show that in the infinite memory limit $M_e \to \infty$ (or $\gamma \to \gamma_F$), the walking speed

remains bounded, and assumes the value

$$\lim_{\gamma\to\gamma_F} u = \frac{\sqrt{2}}{k_F T_d}\left(1-\frac{\gamma_W}{\gamma_F}\right) = \sqrt{\frac{F}{Dk_F T_F}} = \sqrt{\frac{mgA}{DT_F}}. \tag{4.4}$$

In reality, the amplitude $A$ depends on $\gamma$ through the phase $\Phi$, so $u$ does not necessarily increase with $\gamma$. Moreover, Moláček & Bush (2013*b*) demonstrate that the walking speed curves such as those in figure 2 may have discontinuities resulting from the drop switching between different walking modes as $\gamma$ increases, an effect that could not be captured with our resonant walker model.

### 4.2. *Wave field*

Plots of the strobed wave field (2.14) generated by a walker moving according to $\boldsymbol{x}_p = (ut, 0)$ are shown in figure 3 for low, medium, and high memory. The plots are shown in the drop's reference frame, with the drop at the origin and moving to the right. Note that, as the memory increases, the interference effects of the standing waves become more pronounced. The computed wave fields are qualitatively similar to those reported by Eddi *et al.* (2011). Profiles of the wave fields along the drop's direction of motion are also shown. Note that the drop is effectively surfing on the crest of its guiding wave. If $\gamma < \gamma_W$, the drop bounces in place ($u = 0$) on the crest of the wave. As the memory increases, the drop slides further down the wave in the direction of increasing gradient, and so moves faster. The horizontal force $-mg\nabla h(\boldsymbol{x}_p, t)$ imparted by the inclined surface precisely balances the drag $-D\dot{\boldsymbol{x}}_p$, allowing the drop to move at a constant speed.

## 5. Stability analysis

Steady rectilinear walking is observed in the laboratory for a substantial range of parameter space (Protière *et al.* 2006; Moláček & Bush 2013*b*), indicating that the walking state is relatively robust. We proceed by showing that the walking solution $\boldsymbol{x}_p = (ut, 0)$ is stable to perturbations in the direction of motion, and neutrally stable to transverse perturbations. To this end, we consider the dimensionless equation

$$\kappa\ddot{\boldsymbol{x}}_p + \dot{\boldsymbol{x}}_p = \beta\int_{-\infty}^{t} \frac{\mathrm{J}_1(|\boldsymbol{x}_p(t)-\boldsymbol{x}_p(s)|)}{|\boldsymbol{x}_p(t)-\boldsymbol{x}_p(s)|}(\boldsymbol{x}_p(t)-\boldsymbol{x}_p(s))\mathrm{e}^{-(t-s)}\,\mathrm{d}s + \epsilon\boldsymbol{\delta}(t), \tag{5.1}$$

where $\boldsymbol{\delta}(t) = (\delta_x(t), \delta_y(t))$ is the Dirac delta function and $0 < \epsilon \ll 1$. The delta function represents a small perturbation to the drop at time $t = 0$, the response to which we examine in what follows.

We write the drop trajectory as $\boldsymbol{x}_p(t) = \boldsymbol{x}_0(t) + \epsilon\boldsymbol{x}_1(t)H(t)$ where $\boldsymbol{x}_0(t) = (ut, 0)$ is the walking solution defined by (4.2) and $\boldsymbol{x}_1(t) = (x_1(t), y_1(t))$ is the perturbation. We impose the conditions $\boldsymbol{x}_1(0) = (0, 0)$ and $\dot{\boldsymbol{x}}_1(0) = (1/\kappa, 1/\kappa)$ to ensure that $\boldsymbol{x}_p$ is a solution of (5.1). We substitute this solution into (5.1) and retain only the $O(\epsilon)$ terms:

$$\kappa\ddot{x}_1 + \dot{x}_1 = \beta\int_{-\infty}^{t} \mathrm{J}_1'(u(t-s))(x_1(t)-x_1(s)H(s))\mathrm{e}^{-(t-s)}\,\mathrm{d}s, \tag{5.2a}$$

$$\kappa\ddot{y}_1 + \dot{y}_1 = \beta\int_{-\infty}^{t} \frac{\mathrm{J}_1(u(t-s))}{u(t-s)}(y_1(t)-y_1(s)H(s))\mathrm{e}^{-(t-s)}\,\mathrm{d}s. \tag{5.2b}$$

Note that these equations can be written in the form

$$\kappa\ddot{x}_1 + \dot{x}_1 = \beta\left[x_1\int_0^{\infty}\mathrm{J}_1'(uz)\mathrm{e}^{-z}\,\mathrm{d}z - x_1 * \left(\mathrm{J}_1'(ut)\mathrm{e}^{-t}\right)\right], \tag{5.3a}$$

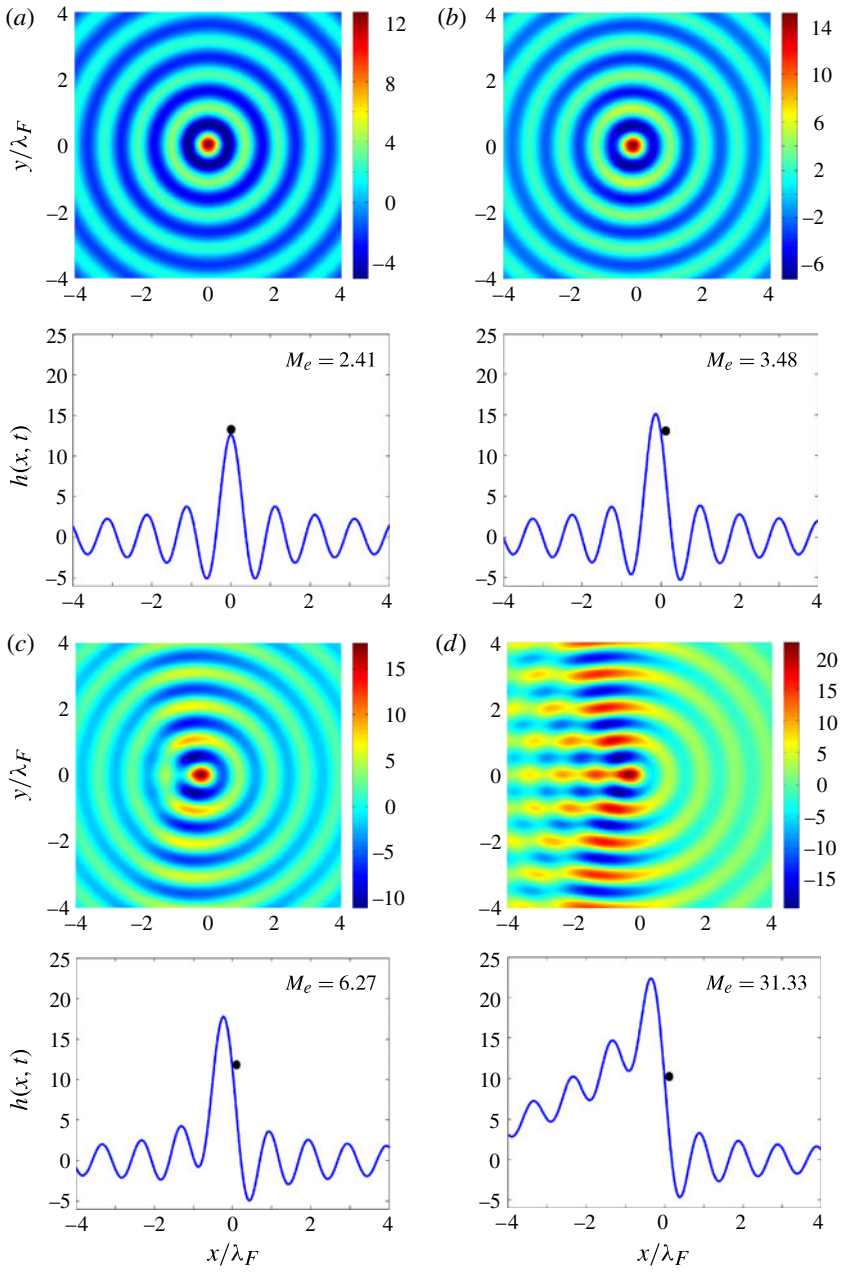


FIGURE 3. Wave fields generated by (*a*) a stationary bouncer and (*b–d*) walkers for, respectively, (*a*) very low ($\gamma = 3.0g$), (*b*) low ($\gamma = 3.4g$), (*c*) medium ($\gamma = 3.8g$), and (*d*) high ($\gamma = 4.2g$) path-memory. The plots are generated using $\nu = 20$ cS, $f = 80$ Hz, $\rho = 949$ kg m$^{-3}$, $\sigma = 20.6 \times 10^{-3}$ N m$^{-1}$, $T_d = 1/54.9$ s, $R = 0.40$ mm, and $\sin\Phi = 0.3$. The walking and Faraday thresholds are $\gamma_W = 3.12g$ and $\gamma_F = 4.3g$, respectively. The wave amplitude is given in μm. Upper figures: plot of the strobed wave field $h(\boldsymbol{x}, t)$ (2.14) accompanying the drop. The drop is located at the origin and moves to the right according to $\boldsymbol{x}_p = (ut, 0)$, where $u$ is determined by (4.3). Lower figures: wave profiles $h(x, t)$ along the direction of motion of the walker. As the memory increases, the walker moves away from the crest towards a region with higher slope, thus moving faster.

$$\kappa\ddot{y}_1 + \dot{y}_1 = \beta\left[y_1\int_0^\infty \frac{\mathrm{J}_1(uz)}{uz}\mathrm{e}^{-z}\,\mathrm{d}z - y_1 * \left(\frac{\mathrm{J}_1(ut)}{ut}\mathrm{e}^{-t}\right)\right], \tag{5.3b}$$

where $f * g$ denotes the convolution of the functions $f$ and $g$. This form of the linearized equations of motion makes them particularly amenable to stability analysis, since we can now take the Laplace transform of both sides of the equations. Doing so yields algebraic equations for $X(s) = \mathscr{L}[x_1(t)]$ and $Y(s) = \mathscr{L}[y_1(t)]$, which can be readily solved. The poles of $X(s)$ and $Y(s)$ are the eigenvalues of their respective linear problems (5.3*a*) and (5.3*b*). If the poles lie in the left- or right-half of the complex plane, the walking solution $\boldsymbol{x}(t) = (ut, 0)$ is respectively stable or unstable to perturbations in the corresponding direction.

### 5.1. *Stability to perturbations in the direction of motion*

We first consider the equation for $x_1$, the perturbation along the walking direction. We take the Laplace transform of the equation and use the facts that $x_1(0) = 0$ and $\dot{x}_1(0) = 1/\kappa$, in order to deduce an equation for $X(s)$:

$$(\kappa s^2 + s)X(s) - 1 = \beta X(s)\int_0^\infty \mathrm{J}_1'(uz)\mathrm{e}^{-z}\,\mathrm{d}z - \beta\mathscr{L}\left[\mathrm{J}_1'(ut)\mathrm{e}^{-t}\right]X(s). \tag{5.4}$$

We now use the facts that

$$\int_0^\infty \mathrm{J}_1'(uz)\mathrm{e}^{-z}\,\mathrm{d}z = \frac{1}{2\sqrt{u^2+1}}\left(1 - \frac{u^2}{\left(1+\sqrt{u^2+1}\right)^2}\right) = \frac{1}{\beta} \tag{5.5a}$$

and

$$\mathscr{L}\left[\mathrm{J}_1'(ut)\mathrm{e}^{-t}\right] = \frac{1}{2\sqrt{u^2+(s+1)^2}}\left(1 - \frac{u^2}{\left(s+1+\sqrt{u^2+(s+1)^2}\right)^2}\right), \tag{5.5b}$$

in order to obtain

$$X(s) = \frac{1}{\kappa s^2 + s - 1 + \dfrac{\beta}{2\sqrt{u^2+(s+1)^2}}\left(1 - \dfrac{u^2}{\left(s+1+\sqrt{u^2+(s+1)^2}\right)^2}\right)}. \tag{5.6}$$

Note that the appropriate branch for the square root is defined by $\sqrt{u^2+(s+1)^2} > 0$ for $s = 0$, with branch cuts $s = -1 \pm \mathrm{i}\xi$ for $\xi \geqslant u$. For simplicity, we write $X(s)$ in terms of the variable $\tilde{s} = s + 1$. After some algebra, we can rewrite (5.6) as

$$X(s) = \frac{\sqrt{u^2+\tilde{s}^2}\left(\tilde{s}+\sqrt{u^2+\tilde{s}^2}\right)}{\kappa(\tilde{s}-1)^2(u^2+\tilde{s}^2) + \beta\tilde{s} + (\tilde{s}-2)(u^2+\tilde{s}^2) + \left[\tilde{s}(\tilde{s}-2) + \kappa\tilde{s}(\tilde{s}-1)^2\right]\sqrt{u^2+\tilde{s}^2}}. \tag{5.7}$$

The poles of $X(s)$ are the zeros of its denominator, which solve the equation

$$[\tilde{s}(\tilde{s}-2) + \kappa\tilde{s}(\tilde{s}-1)^2]\sqrt{u^2+\tilde{s}^2} = (2-\tilde{s})(\tilde{s}^2+u^2) - \beta\tilde{s} - \kappa(\tilde{s}-1)^2(\tilde{s}^2+u^2). \tag{5.8}$$

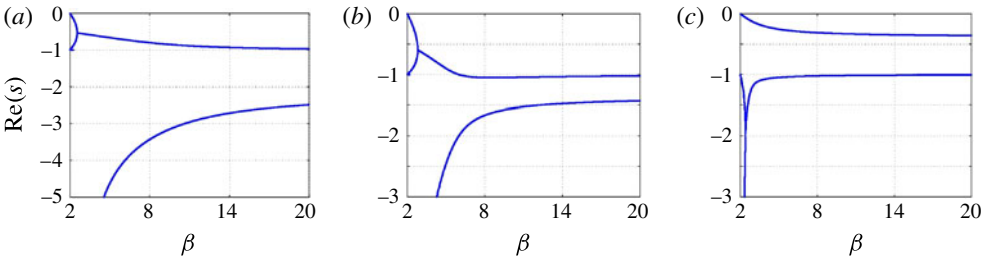


FIGURE 4. (Colour online) Plot of the real part of the (non-zero) poles of $\mathscr{L}[x_1(t)] = X(s)$ as a function of $\beta$, for (*a*) $\kappa = 1$, (*b*) $\kappa = 1.5$ and (*c*) $\kappa = 5$, respectively. $X(s)$ is the Laplace transform of the perturbation $x_1$, $\beta$ the non-dimensional memory force coefficient, and $\kappa$ the non-dimensional mass of the drop (see table 1). The three plots are representative of the ranges $0 \leqslant \kappa \lesssim 1.3$, $1.3 \lesssim \kappa < 2$, and $\kappa > 2$, respectively. Note that merging of the curves indicates the existence of two complex conjugate poles with the same real part.

Squaring both sides of this equation and some further algebra yields

$$[u^2(\tilde{s} - 2 + \kappa(\tilde{s} - 1)^2)^2 + 2\beta\tilde{s}(\tilde{s} - 2 + \kappa(\tilde{s} - 1)^2)](\tilde{s}^2 + u^2) = -\beta^2\tilde{s}^2. \tag{5.9}$$

Note that the poles of $X(s)$ are a subset of the solutions to this equation, since squaring both sides may introduce spurious solutions; that is, some solutions of (5.9) may not solve (5.8). Therefore, the poles of $X(s)$ are a subset of the roots of the sixth-degree polynomial $p_x(\tilde{s}) = \sum_{k=0}^{6} c_k \tilde{s}^k$, with coefficients

$$c_0 = 4u^4\left(1 - \kappa + \frac{\kappa^2}{4}\right), \quad c_1 = -u^2\left[4\beta + 4u^2 + \kappa(-2\beta - 10u^2 + 4\kappa u^2)\right], \tag{5.10a}$$

$$c_2 = \beta^2 + 4u^2 + 2\beta u^2 + u^4 + \kappa\left(-4u^2 - 4\beta u^2 - 8u^4 + \kappa u^2 + 6\kappa u^4\right), \tag{5.10b}$$

$$c_3 = -\left[4\beta + 4u^2 + \kappa\left(-2\beta - 10u^2 - 2\beta u^2 - 2u^4 + 4\kappa u^2 + 4\kappa u^4\right)\right], \tag{5.10c}$$

$$c_4 = u^2 + 2\beta + \kappa\left(-4\beta - 8u^2 + 6\kappa u^2 + \kappa u^4\right), \tag{5.10d}$$

$$c_5 = \kappa(2\beta + 2u^2 - 4\kappa u^2), \quad c_6 = \kappa^2 u^2. \tag{5.10e}$$

It can be verified that $p_x(1) = 0$, so $X(s)$ has a pole at the origin $s = 0$. This reflects the fact that the equation of motion (3.1) is invariant under translation in the $x$ direction; that is, if $\boldsymbol{x}_p(t)$ is a solution to (3.1), so is $\boldsymbol{x}_p(t) + (\tilde{x}, 0)$, where $\tilde{x}$ is a constant. Since $\mathscr{L}[\tilde{x}] = \tilde{x}/s$, the translational invariance of the solution implies that $X(s)$ has a pole at $s = 0$ (or $\tilde{s} = 1$). Therefore, the non-trivial poles of $X(s)$ are a subset of the roots of the fifth-degree polynomial $q_x(\tilde{s}) = \sum_{k=0}^{5} d_k \tilde{s}^k$, where $p_x(\tilde{s}) = (\tilde{s} - 1)q_x(\tilde{s})$. The coefficients of $q_x(\tilde{s})$ are related to the coefficients of $p_x(\tilde{s})$ by the formula $d_i = -\sum_{k=0}^{i} c_k$.

We find the roots of $q_x(\tilde{s})$ numerically with MATLAB for a range of parameters $\beta$ and $\kappa$, and only select the roots that are actually poles of $X(s)$, that is, solutions of (5.8). The real parts of the roots are plotted in figure 4 for a range of parameters $\kappa$ and $\beta > 2$. Note that the poles of $X(s)$ always have negative real part, indicating that the walking solution $\boldsymbol{x}_p(t) = (ut, 0)$ is stable to perturbations along the direction of motion. That is, if the drop is infinitesimally perturbed along its walking direction, it will converge exponentially quickly to a solution of the form $\boldsymbol{x}_p(t) = (ut + \epsilon\tilde{x}, 0)$. It will thus continue to walk along the same line at the same constant speed.

### 5.2. *Stability to lateral perturbations*

We now show that the walking drop with trajectory $\boldsymbol{x}_p(t) = (ut, 0)$ is neutrally stable to perturbations in the $y$ direction, that is, perpendicular to its direction of motion. Taking the Laplace transform of the $y_1$-equation (5.3*b*) and using the fact that $y_1(0) = 0$ and $\dot{y}_1(0) = 1/\kappa$ yields an algebraic equation for $Y(s) = \mathscr{L}[y_1(t)]$:

$$(\kappa s^2 + s)Y(s) - 1 = \beta Y(s) \int_0^\infty \frac{\mathrm{J}_1(uz)}{uz} \mathrm{e}^{-z}\, \mathrm{d}z - \beta \mathscr{L}\left[\frac{\mathrm{J}_1(ut)}{ut}\mathrm{e}^{-t}\right] Y(s). \tag{5.11}$$

We now use the facts that

$$\int_0^\infty \frac{\mathrm{J}_1(uz)}{uz} \mathrm{e}^{-z}\, \mathrm{d}z = \frac{1}{u^2}\left(-1 + \sqrt{1+u^2}\right) = \frac{1}{\beta}\sqrt{1+u^2}, \tag{5.12a}$$

and

$$\mathscr{L}\left[\frac{\mathrm{J}_1(ut)}{ut}\mathrm{e}^{-t}\right] = \frac{1}{u}\left(-\frac{s+1}{u} + \sqrt{1 + \left(\frac{s+1}{u}\right)^2}\right), \tag{5.12b}$$

to deduce the solution

$$Y(s) = \frac{1}{\kappa s^2 + s - \sqrt{1+u^2} + \dfrac{\beta}{u^2}\left(-(s+1) + \sqrt{u^2 + (s+1)^2}\right)}, \tag{5.13}$$

where the square root has the same meaning as before. Using (4.2) for the walking speed $u$ allows us to rewrite $Y(s)$ as

$$Y(s) = \frac{-1 + 2\beta - \beta^*}{\kappa s^2\left(-1 + 2\beta - \beta^*\right) - s\left(1 + \beta^*\right) + \beta\left(1 - \beta^*\right) + \beta\sqrt{\left(-1+\beta^*\right)^2 + 4s(s+2)}}, \tag{5.14}$$

where $\beta^* = \sqrt{1 + 4\beta}$. As previously, the poles of $Y(s)$ are the zeros of its denominator, which are solutions to

$$\beta\sqrt{\left(-1+\beta^*\right)^2 + 4s(s+2)} = \beta\left(\beta^* - 1\right) + s\left(1 + \beta^*\right) - \kappa s^2\left(-1 + 2\beta - \beta^*\right). \tag{5.15}$$

Squaring both sides of this equation and subsequent algebra yields

$$s^2(1 + 2\beta + \beta^*) = \kappa^2 s^4\left(-1 + 2\beta - \beta^*\right) - 2\kappa s^3\left(1 + \beta^*\right) - 2\kappa s^2\beta\left(-1 + \beta^*\right). \tag{5.16}$$

Therefore, the poles of $Y(s)$ are a subset of the roots of the polynomial $p_Y(s) = s^2(c_0 + c_1 s + c_2 s^2)$, with coefficients

$$c_0 = -\left[2\kappa\beta\left(-1 + \beta^*\right) + 1 + 2\beta + \beta^*\right], \tag{5.17a}$$

$$c_1 = -2\kappa\left(1 + \beta^*\right), \quad c_2 = \kappa^2\left(-1 + 2\beta - \beta^*\right). \tag{5.17b}$$

Note that $p_Y(s)$ has a double zero at the origin $s = 0$, as well as the two roots of $c_0 + c_1 s + c_2 s^2$. However, one can show numerically that these roots do not solve (5.15), and hence they are not poles of $Y(s)$. As a result, $Y(s)$ has only a double pole at the origin, so the drop is neutrally stable with respect to perturbations perpendicular to the direction of motion.

Since the equation of motion (3.1) is invariant under translation in the $y$ direction, we expect a pole at the origin. The double pole, which arises from the rotational

invariance of the problem, indicates that the perturbation $y_1$ grows linearly in time, rather than exponentially. Physically, this indicates that the drop can change direction when perturbed perpendicular to its walking direction. Note that the waves emitted by the drop have radial symmetry, and that the drop is effectively surfing on the central crest of its pilot wave field (figure 3). Hence, there is no force to stabilize the drop to lateral perturbations, so its direction of motion can be readily altered. However, once so perturbed, it will simply walk at a constant speed in the new direction.

## 6. Discussion

We have developed and analysed an integro-differential trajectory equation to describe the horizontal motion of a droplet walking in resonance on a vibrating fluid bath. The equation was developed by approximating the resonant walker as a continuous moving source of standing waves. The resulting theoretical model makes predictions that are consistent with many of the experimental results reported by Protière *et al.* (2006) and Moláček & Bush (2013*b*). Specifically, it predicts that the bouncing state becomes unstable at a critical value of the memory parameter $M_e$ consistent with that observed experimentally. By deriving a Stuart–Landau equation for the motion of the drop near this critical value, we have shown that the bouncing state destabilizes into straight-line walking $\boldsymbol{x}_p = (ut, 0)$ via a supercritical pitchfork bifurcation. The trajectory equation also yields an analytical expression (4.3) for the dependence of the walking speed $u$ on the forcing acceleration $\gamma$ that compares favourably with the experimental results reported by Moláček & Bush (2013*b*).

We have also analysed the stability of the resonant walking state. By demonstrating that the walker is stable to perturbations in the direction of motion, we have provided a new rationale for the robustness of the resonant walking state. By demonstrating that the walker is neutrally stable to perturbations perpendicular to the direction of motion, we provide evidence that the dynamics may be chaotic in more complicated geometries. In the presence of boundaries, the walkers are easily diverted; indeed, steady rectilinear walking is rarely observed in confined geometries (Harris *et al.* 2013), as the wave field is complicated by reflections from the boundaries. The drop trajectory is then extremely sensitive to its initial conditions, which may result in chaotic dynamics. Rationalizing how the coherent statistical behaviour (Couder & Fort 2006; Harris *et al.* 2013) emerges from the underlying complex nonlinear dynamics is a subject of ongoing research.

It is worth stressing that the stroboscopic approximation assumes *a priori* that the droplet and accompanying wave are in a state of perfect resonance. While this resonance assumption greatly simplifies the mathematical analysis, the model does not consider the detailed coupling between the horizontal and vertical drop motion, an important aspect of the dynamics that one expects to have significant bearing on the stability characteristics of the walkers. In particular, the model fails to capture the experimental observations that the walking state is sometimes unstable for sufficiently small or large drops (Moláček & Bush 2013*b*; Wind-Willassen *et al.* 2013), that large drops can undergo a subcritical transition to walking (Protière *et al.* 2006), and that the walking speed of some drops is a non-monotonic or even discontinuous function of the forcing acceleration, owing to the switching between two resonant bouncing modes (Moláček & Bush 2013*b*).

Another limitation of the trajectory equation (3.1) is that it only applies in free space; that is, the fluid bath must be large compared to the damping length of the Faraday and transient wave fields, so that the boundaries and reflected waves can be

safely neglected. Specifically, the Bessel function approximation (2.8) for the standing wave field generated by a single bounce will no longer be valid if the drop is near a submerged barrier or the container boundary. As many of the interesting quantum analogues such as tunnelling (Eddi *et al.* 2009), diffraction and interference (Couder & Fort 2006) occur in the presence of submerged barriers, the incorporation of boundary effects into the pilot-wave model developed herein will be the subject of future work.

While analysing the stability of resonant straight-line walking is informative, the real value of the trajectory equation will be in elucidating certain aspects of the walkers' quantum-like behaviour. In the future, we will show that our trajectory equation can be simply extended to include a Coriolis force, allowing us to elucidate the orbital quantization reported by Fort *et al.* (2010) and to predict qualitatively new phenomena (Harris & Bush 2013; Oza *et al.* 2013). Our model can incorporate central force fields in a similar fashion, thus allowing us to analyse the hydrodynamic analogue of the quantum harmonic oscillator, which is currently being explored in the laboratory of Yves Couder (Perrard *et al.* 2013).

## Acknowledgements

A.U.O. gratefully acknowledges the financial support of the NSF Graduate Research Fellowship Program and the Hertz Foundation, and J.W.M.B. that of the NSF through grant CBET-0966452. The work of R.R.R. was partially supported by NSF grants DMS-1007967 and DMS-1115278. The authors also thank J. Moláček, D. Harris, Y. Couder and E. Fort for valuable discussions, and the MIT-France program for their support.

## REFERENCES

BENJAMIN, T. B. & URSELL, F. 1954 The stability of the plane free surface of a liquid in vertical periodic motion. *Proc. R. Soc.* A **225**, 505–515.

BUSH, J. W. M. 2010 Quantum mechanics writ large. *Proc. Natl Acad. Sci. USA* **107** (41), 17455–17456.

COUDER, Y. & FORT, E. 2006 Single-particle diffraction and interference at a macroscopic scale. *Phys. Rev. Lett.* **97**, 154101.

COUDER, Y., GAUTIER, C.-H. & BOUDAOUD, A. 2005 From bouncing to floating: noncoalescence of drops on a fluid bath. *Phys. Rev. Lett.* **94**, 177801.

CROMMIE, M., LUTZ, C. & EIGLER, D. 1993 Confinement of electrons to quantum corrals on a metal surface. *Science* **262** (5131), 218–220.

DOUADY, S. 1990 Experimental study of the Faraday instability. *J. Fluid Mech.* **221**, 383–409.

EDDI, A., FORT, E., MOISY, F. & COUDER, Y. 2009 Unpredictable tunneling of a classical wave–particle association. *Phys. Rev. Lett.* **102**, 240401.

EDDI, A., MOUKHTAR, J., PERRARD, S., FORT, E. & COUDER, Y. 2012 Level splitting at macroscopic scale. *Phys. Rev. Lett.* **108**, 264503.

EDDI, A., SULTAN, E., MOUKHTAR, J., FORT, E., ROSSI, M. & COUDER, Y. 2011 Information stored in Faraday waves: the origin of path memory. *J. Fluid Mech.* **675**, 433–463.

EDDI, A., TERWAGNE, D., FORT, E. & COUDER, Y. 2008 Wave propelled ratchets and drifting rafts. *Europhys. Lett.* **82**, 44001.

FARADAY, M. 1831 On a peculiar class of acoustical figures, and on certain forms assumed by groups of particles upon vibrating elastic surfaces. *Phil. Trans. R. Soc. Lond.* **121**, 299–340.

FORT, E., EDDI, A., BOUDAOUD, A., MOUKHTAR, J. & COUDER, Y. 2010 Path-memory induced quantization of classical orbits. *Proc. Natl Acad. Sci. USA* **107** (41), 17515–17520.

HARRIS, D. M. & BUSH, J. W. M. 2013 Droplets walking in a rotating frame: from quantized orbits to multinodal statistics. *J. Fluid Mech.* (submitted).

HARRIS, D. M., MOUKHTAR, J., FORT, E., COUDER, Y. & BUSH, J. W. M. 2013 Wavelike statistics from pilot-wave dynamics in a circular corral. *Phys. Rev.* E **88**, 011001.

KUMAR, K. 1996 Linear theory of Faraday instability in viscous fluids. *Proc. R. Soc.* A **452**, 1113–1126.

MILES, J. & HENDERSON, D. 1990 Parametrically forced surface waves. *Annu. Rev. Fluid Mech.* **22**, 143–165.

MOLÁČEK, J. & BUSH, J. W. M. 2013*a* Drops bouncing on a vibrating bath. *J. Fluid Mech.* **727**, 582–611.

MOLÁČEK, J. & BUSH, J. W. M. 2013*b* Drops walking on a vibrating bath: towards a hydrodynamic pilot-wave theory. *J. Fluid Mech.* **727**, 612–647.

MÜLLER, H. W., FRIEDRICH, R. & PAPATHANASSIOU, D. 1998 Theoretical and experimental investigations of the Faraday instability. In *Evolution of Spontaneous Structures in Dissipative Continuous Systems* (ed. F. Busse & S. C. Müller), Lecture Notes in Physics, vol. 55, pp. 231–265. Springer.

OZA, A. U., HARRIS, D. M., ROSALES, R. R. & BUSH, J. W. M. 2013 Pilot-wave dynamics in a rotating frame: on the emergence of orbital quantization. *J. Fluid Mech.* (submitted).

PERRARD, S., LABOUSSE, M., MISKIN, M., FORT, E. & COUDER, Y. 2013 Macroscopic wave–particle eigenstates. Under review.

PROSPERETTI, A. 1976 Viscous effects on small-amplitude surface waves. *Phys. Fluids* **19** (2), 195–203.

PROTIÈRE, S., BOUDAOUD, A. & COUDER, Y. 2006 Particle–wave association on a fluid interface. *J. Fluid Mech.* **554**, 85–108.

SHIROKOFF, D. 2013 Bouncing droplets on a billiard table. *Chaos* **23**, 013115.

STUART, J. T. 1958 On the nonlinear mechanics of hydrodynamic stability. *J. Fluid Mech.* **4**, 1–21.

WALKER, J. 1978 Drops of liquid can be made to float on the liquid. What enables them to do so? *Sci. Am.* **238-6**, 151–158.

WIND-WILLASSEN, Ø., MOLÁČEK, J., HARRIS, D. M. & BUSH, J. W. M. 2013 Exotic states of bouncing and walking droplets. *Phys. Fluids* **25**, 082002.